

Article

Synthesis, Structure and Binding Properties of Lipophilic Cavitands based on a Calix[4]pyrrole-Resorcinarene Hybrid Scaffold

Albano Galan, Eduardo C. Escudero-Adán, Antonio Frontera, and Pablo Ballester

J. Org. Chem., **Just Accepted Manuscript** • DOI: 10.1021/jo5007224 • Publication Date (Web): 20 May 2014

Downloaded from <http://pubs.acs.org> on May 26, 2014

Just Accepted

"Just Accepted" manuscripts have been peer-reviewed and accepted for publication. They are posted online prior to technical editing, formatting for publication and author proofing. The American Chemical Society provides "Just Accepted" as a free service to the research community to expedite the dissemination of scientific material as soon as possible after acceptance. "Just Accepted" manuscripts appear in full in PDF format accompanied by an HTML abstract. "Just Accepted" manuscripts have been fully peer reviewed, but should not be considered the official version of record. They are accessible to all readers and citable by the Digital Object Identifier (DOI®). "Just Accepted" is an optional service offered to authors. Therefore, the "Just Accepted" Web site may not include all articles that will be published in the journal. After a manuscript is technically edited and formatted, it will be removed from the "Just Accepted" Web site and published as an ASAP article. Note that technical editing may introduce minor changes to the manuscript text and/or graphics which could affect content, and all legal disclaimers and ethical guidelines that apply to the journal pertain. ACS cannot be held responsible for errors or consequences arising from the use of information contained in these "Just Accepted" manuscripts.



ACS Publications
High quality. High impact.

The Journal of Organic Chemistry is published by the American Chemical Society.
1155 Sixteenth Street N.W., Washington, DC 20036
Published by American Chemical Society. Copyright © American Chemical Society.
However, no copyright claim is made to original U.S. Government works, or works
produced by employees of any Commonwealth realm Crown government in the course
of their duties.

Synthesis, Structure and Binding Properties of Lipophilic Cavitands based on a Calix[4]pyrrole- Resorcinarene Hybrid Scaffold

Albano Galán,[‡] Eduardo C. Escudero-Adán,[†] Antonio Frontera,[#] and Pablo Ballester^{,‡,§}*

[‡] Institute of Chemical Research of Catalonia (ICIQ), Avgda. Països Catalans 16, 43007 Tarragona,
Spain

[†] X-ray Diffraction Unit, Institute of Chemical Research of Catalonia (ICIQ), Avgda. Països Catalans
16, 43007 Tarragona, Spain

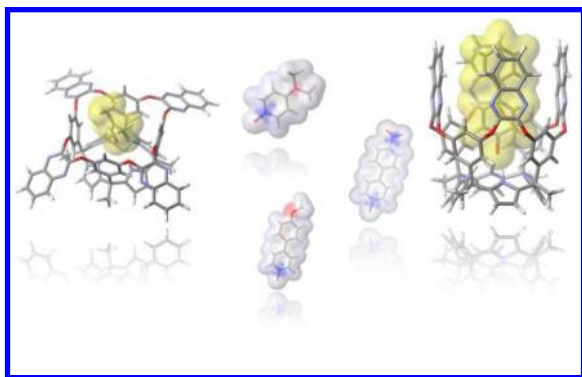
[§] Catalan Institution for Research and Advanced Studies (ICREA), Passeig Lluís Companys, 23, 08010
Barcelona, Spain

[#] Departament de Química, Universitat de les Illes Balears, Crta. Valldemossa Km. 7.5, 07122- Palma,
Spain

pballerster@iciq.es

**RECEIVED DATE (to be automatically inserted after your manuscript is accepted if required
according to the journal that you are submitting your paper to)**

SYNOPSIS TOC



ABSTRACT

We report the synthesis, structural characterization and binding properties of a series of unprecedented cavitands based on a *meso*-dodecyl-calix[4]pyrrole-resorcin[4]arene hybrid scaffold. The reported structural and conformational features of the prepared cavitands are derived from results obtained in solution, solid state and molecular modeling studies. In the solid state, these cavitands are exclusively observed in the kite C_4 structure and as racemic mixture of two cyclochiral conformers, which are interconverting fast on the ^1H NMR timescale, according to solution studies. In agreement, molecular modeling studies assign an energy preference for the kite conformer of the cavitands. The polar interior of the synthesized containers allows for the inclusion of a series of pyridine *N*-oxide derivatives. This results in the formation of 1:1 complexes that are kinetically and thermodynamically highly stable. The putative switching process between the vase and kite forms of these cavitands is investigated in solution by means of variable temperature ^1H NMR experiments. *N*-oxide guests that are size and shape complementary to the volume of the cavity of the vase form are also employed to facilitate its emergence. All the results obtained indicate the existence of a remarkable preference toward the kite conformation both in free and bound calix[4]pyrrole-based cavitands.

INTRODUCTION

Cavitands are synthetic molecules that contain an intrinsic cavity capable of including sizeable guests (molecules or ions).¹ In this sense, the elaboration of the shallow cavity provided by the cone conformer

of resorcin[4]arene **1** through the incorporation of aromatic panels at its upper rim constitutes a valuable synthetic strategy for the construction of deep cavitands.^{1,2,3,4} The upper rim functionalization of **1** is easily accessible synthetically due to the presence of the eight hydroxyl groups. The construction of deeper cavities has the dual effect of increasing the shielding of bound guests from the solvent and restricting the conformational flexibility of the initial resorcinarene scaffold. In addition, extending the cavity of a receptor molecule may confer new binding properties or modulate its kinetic and thermodynamic binding features.⁵ Examples of functional deep cavitands based on multiply bridged resorcin[4]arene structures are abundant in literature.⁶ These compounds have been extremely useful both in the self-assembly of molecular capsules^{7,8} and in the construction of covalent cages.⁹ Supramolecular sensors,¹⁰ catalysts¹¹ or even molecular grippers^{12,13} have also been derived from resorcinarene based cavitands. Unfortunately, the extensive use of aromatic panels to shape and elaborate the cavity in resorcinarene based deep cavitands renders their interiors deprived from polar functional groups. Nevertheless, attempts to functionalize the interiors of resorcinarene based deep cavitands with one carboxylic group^{14,15,16} or several pyrrole units¹⁷ have been reported.

Calix[4]pyrroles are tetrapyrrolic macrocyclic compounds known to act as effective receptors for anions and electron rich neutral compounds.¹⁸ The substitution at each of the four *meso* positions of the calix[4]pyrrole core by a phenyl group affords aryl-extended calix[4]pyrroles containing deep cavities defined by fixed aromatic walls.¹⁹ In 2007, our group reported the synthesis of the $\alpha,\alpha,\alpha,\alpha$ -isomer of aryl-extended calix[4]pyrrole **2a** decorated with eight hydroxyl groups at its upper rim (Figure 1).²⁰ The structure of **2a** reminded us of resorcinarene **1** and was described as a resorcinarene-calix[4]pyrrole hybrid. We envisioned that calix[4]pyrrole-resorcinarene hybrid **2a** could be a suitable scaffold for the construction of deep cavitands functionalized with four pyrrole units at their closed ends. Our expectations were that the synthetic strategies used in the preparation of deep cavitands derived from resorcin[4]arene **1** could be directly applied to further elaborate the aromatic cavity of **2**. Most of these synthetic strategies involved the bridging of vicinal hydroxyl groups at the upper rim with suitable aromatic spacers. To the best of our knowledge, there is only one example of cavitands derived from

aryl-extended calix[4]pyrrole scaffolds in literature.²¹ However, the described compounds do not qualify as deep cavitands. Their structures correspond to doubly bridged phosphonated cavitands derived from a tetraol aryl extended calix[4]pyrrole. These compounds are reminiscent of the phosphonate-calix[4]arene cavitands of Dalcanele^{22,23,24} and Dutasta.^{25,26} Here, we describe the synthesis of a series of tetrabridged deep cavitands derived from calix[4]pyrrole hybrid **2b**. We also report the conformational properties of the synthesized cavitands, both in solution and in solid state. Finally, we discuss the experimental results of the binding studies of these novel cavitands with pyridine *N*-oxide derivatives.

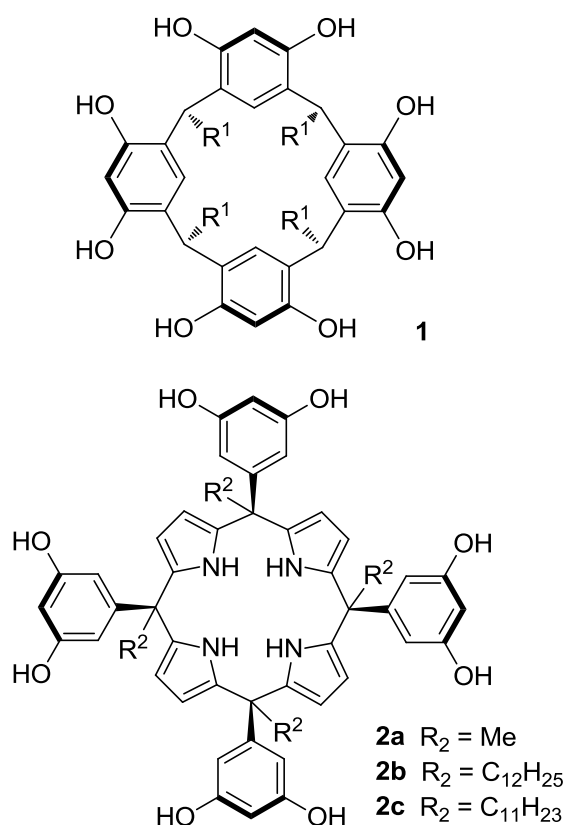
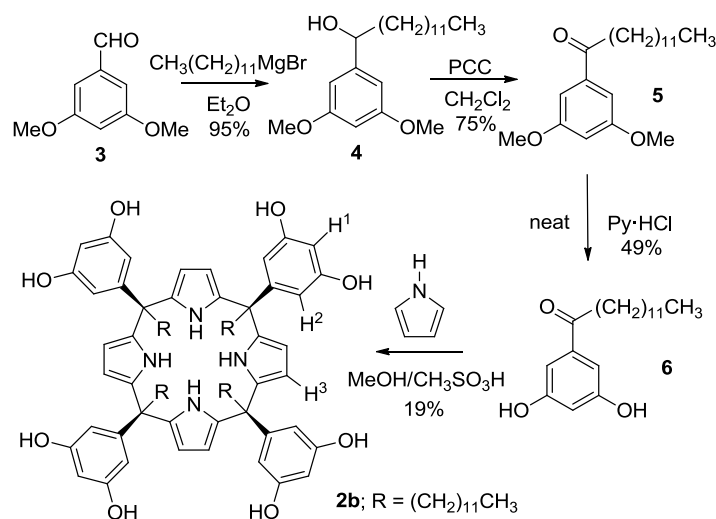


Figure 1. Molecular structures of resorcin[4]arene **1** and calix[4]pyrrole-resorcin[4]arene hybrid **2**.

RESULTS AND DISCUSSION

Synthesis of lipophilic calix[4]pyrrole-resorcin[4]arene hybrid 2b. All synthetic attempts to elongate the cavity of built-in calix[4]pyrrole **2a** led to reaction mixtures with low solubility in most common organic solvents. The limited solubility of the crude reaction product made the analysis of the mixture

and its purification troublesome. To overcome this limitation, we decided to use the more lipophilic calix[4]pyrrole derivative **2b** as the initial building block. Calix[4]pyrrole **2b** is a structural analog to **2c** but contains an extra carbon atom in its *meso*-alkyl chains. A synthetic procedure for calix[4]pyrrole **2c** was recently reported by Cohen.²⁷ Inspired by the reported synthetic methodology, we prepared dodecyl-3,5-dihydroxy-phenyl ketone **6** in 3 steps. The nucleophilic addition of dodecyl magnesium bromide to 3,5-dimethoxybenzaldehyde **3** afforded the benzylic alcohol **4** in 95% yield. Oxidation of alcohol **4** with PCC provided ketone **5**, which was demethylated with molten pyridinium chloride affording the dihydroxyphenyl-dodecyl ketone **6** in 14% overall yield. Finally, the acid catalyzed condensation of phenyl ketone **6** with pyrrole afforded, after column chromatography purification and crystallization from acetonitrile, the calixpyrrole-resorcinarene hybrid **2b** as a white solid in 19% yield.



Scheme 1. Synthetic scheme for the preparation of the calix[4]pyrrole-resorcin[4]arene hybrid **2b**.

As shown in Figure 2, the ^1H NMR spectrum of **2b** in CDCl_3 solution shows broad proton signals. We assume that similarly to the reported findings for **2c** this is mainly due to aggregation phenomena. Conversely, in polar organic solvents that disrupt intermolecular hydrogen-bonding interactions, like $\text{MeOH}-d_4$ or $\text{THF}-d_8$, the ^1H -NMR spectrum of **2b** shows sharp and well-defined proton signals.

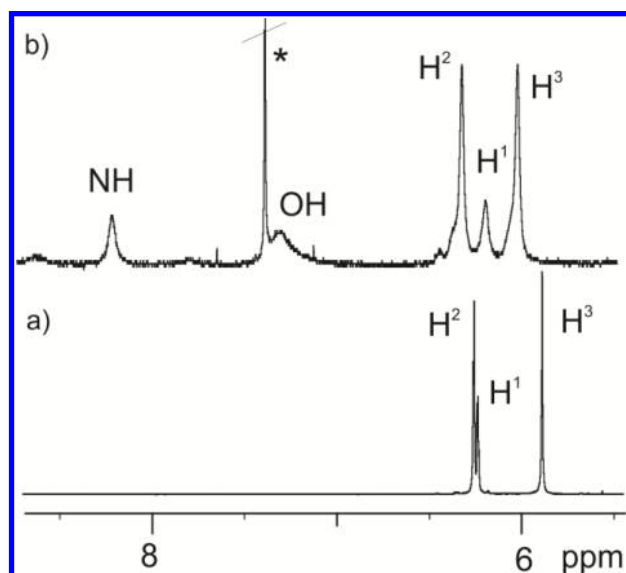


Figure 2. Selected downfield region of ^1H NMR spectra of 10 mM solutions of calixpyrrole **2b** a) in $\text{MeOH-}d_4$ and b) in CDCl_3 . * Residual peak of non-deuterated solvents. See Scheme 1 for proton assignment.

Single crystals of **2b** suitable for X-ray diffraction were grown from an acetonitrile solution. The analysis of the diffraction data revealed that in the solid state calixpyrrole **2b** adopts the cone conformation and features one molecule of acetonitrile included in its aromatic cavity. The cone conformation of **2b** is stabilized by the formation of intramolecular hydrogen bonds between the hydroxyl groups at its upper rim. In addition, the included acetonitrile molecule is hydrogen bonded simultaneously to the four convergent pyrrolic NHs of **2b**. The binding geometry of the solvate $\text{CH}_3\text{CN}\cdot\text{2b}$ is a key factor in stabilizing the calix[4]pyrrole core in the cone conformation. The averaged $\text{N}\cdots\text{N}$ distance of the four hydrogen-bonds is 3.22 Å. The acetonitrile solvate $\text{CH}_3\text{CN}\cdot\text{2b}$ packs into rows through the intermediacy of water molecules that are hydrogen bonded to two adjacent solvates in the same row.

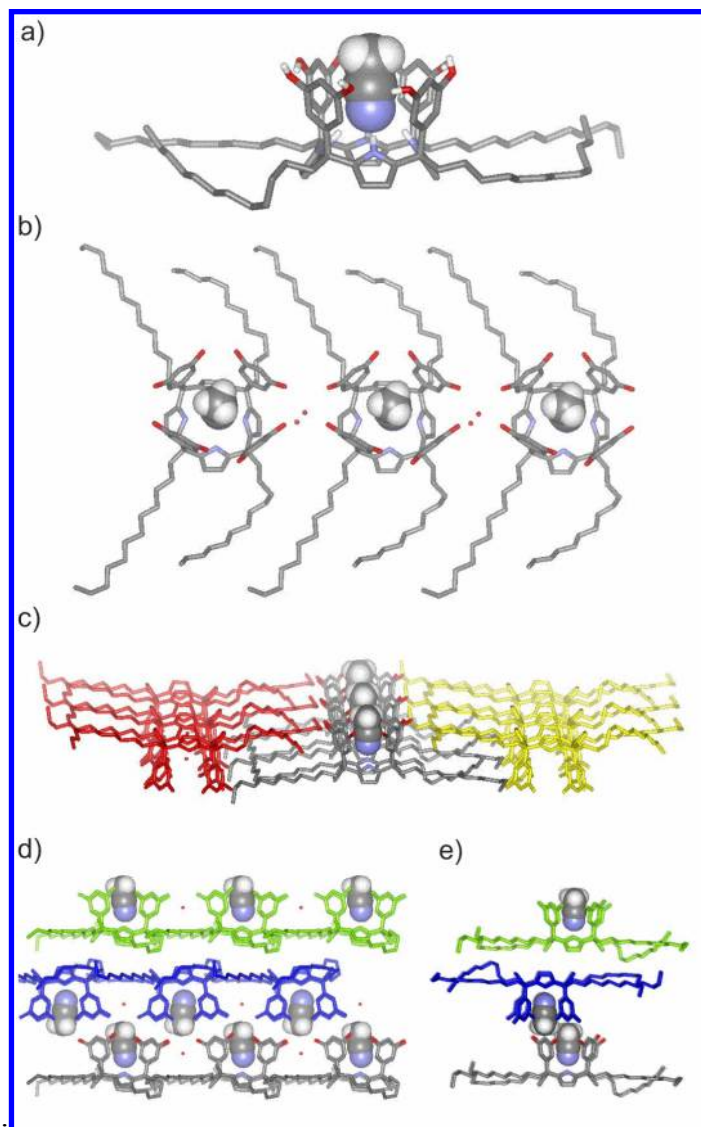


Figure 3. a) X-ray structure of the solvate $\text{CH}_3\text{CN}\cdot\mathbf{2b}$; b) adjacent solvates of $\text{CH}_3\text{CN}\cdot\mathbf{2b}$ form rows; c) three rows of adjacent $\text{CH}_3\text{CN}\cdot\mathbf{2b}$ solvates pack to form a layer with the polar heads directed in opposite directions; d) side and e) front views of the bilayers resulting from the packing of layers of solvates. For clarity, non-polar hydrogen atoms are removed in a) and all hydrogen atoms in b), c) and d). Selected acetonitrile molecules are shown as CPK models and $\mathbf{2b}$ is depicted in stick representation.

The *meso*-alkyl substituents (tails) belonging to adjacent $\text{CH}_3\text{CN}\cdot\mathbf{2b}$ complexes are involved in van-der-Waals interactions. Each row of $\text{CH}_3\text{CN}\cdot\mathbf{2b}$ solvates is flanked by two analogous parallel rows with the polar upper rims (head) of $\mathbf{2b}$ oriented in opposite directions. This arrangement of rows forms a layer with alternating lipophilic and hydrophilic strips. Layers pack on top of each other by confronting

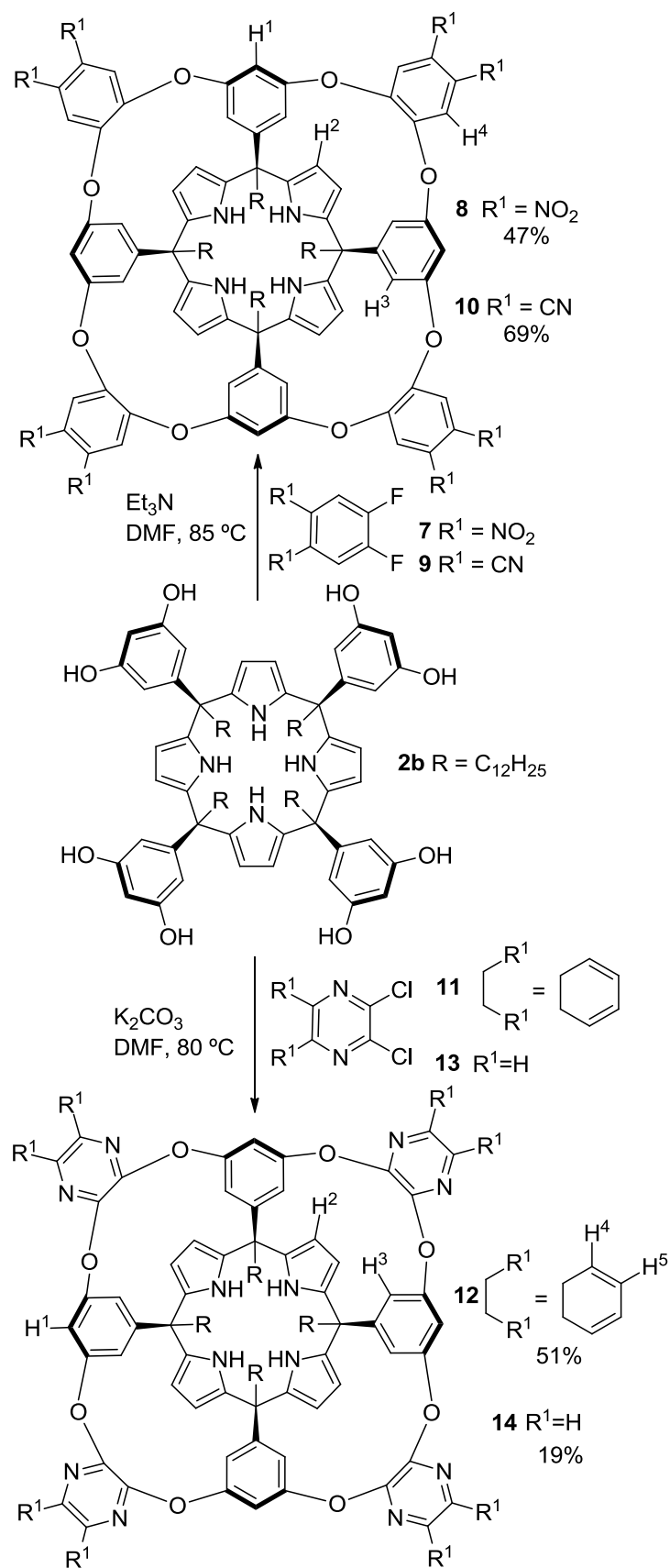
strips of the same polarity. Thus, head-to-head interactions between $\text{CH}_3\text{CN} \subset \mathbf{2b}$ solvates in different layers are promoted through water-mediated hydrogen bonding interactions while tail-to-tail contacts are mainly of van-der-Waals nature. Each molecule of **2b** is involved in head-to-head interactions with two other molecules of **2b** pertaining to two contiguous rows of an adjacent layer. Acetonitrile molecules fill the voids produced in the described packing. The crystal packing demonstrates the existence of bilayers of calixpyrrole molecules **2b**, in which the polar and non-polar sections segregate. This result highlights the amphiphilic character of **2b**.

Synthesis of calix[4]pyrrole based deep cavitands. The construction of deep cavitands based on resorcin[4]arene **1** relies in the elaboration of its aromatic cavity by incorporation of four aromatic flaps at its upper rim. The additional aromatic flaps are easily introduced through nucleophilic aromatic substitution reactions between the hydroxyl groups at the upper rim of **1** and *ortho*-disubstituted fluoro and chloro electron-deficient six-membered aromatic and hetero-aromatic rings.²⁸

Using analogous synthetic procedures to the ones applied for the elaboration of the cavity of **1**, we set out to synthesize deep cavitands derived from the calix[4]pyrrole-resorcin[4]arene hybrid **2b**. The reaction of hybrid **2b** with 4 equivalents of *ortho*-1,2-difluoro-4,5-dinitro benzene **7** carried out by heating a dimethylformamide (DMF) solution at 85 °C in the presence of an excess of triethylamine afforded, after column chromatography purification, the four-folded bridged cavitand **8** as a yellow solid (mp > 251 °C, decomp) in 47 % yield. We did not detect the presence of partially (reacted) bridged products in the reaction mixture.

Similarly, the reaction of **2b** with 1,2-difluoro-4,5-dicyano benzene **9** produced octanitrile calix[4]pyrrole cavitand **10** as a white solid (mp > 292 °C, decomp) in 69% yield (Scheme 3).

The synthesis of cavitands **12** and **14** required the modification of the reaction conditions. Thus, **2b** was reacted with 4 equivalents of 2,3-dichloroquinoxaline **11** using potassium carbonate as a base in DMF. After purification of the crude reaction, cavitand **12** was isolated as a white solid in a 51% yield (mp > 328 °C, decomp). Analogously, the reaction of 2,3-dichloro-1,4-pyrazine **13** with **2b** afforded cavitand **14** as a white solid (mp > 275 °C, decomp) in 12% yield.



Scheme 2. Synthetic schemes for the preparation of deep cavitands **8**, **10**, **12** and **14**.

Structures of the vase and kite conformers of calix[4]pyrrole based deep cavitands, thermodynamic stabilities and interconversion processes.

Molecular modeling studies indicate that in cavitands **8**, **10**, **12**, and **14** the base of four phenyl rings, which are connected at the *meso* positions of the calix[4]pyrrole unit, and the four fifteen-membered rings formed an enforced concave cavity closed at one end by the four pyrrole rings. Regardless of the starting geometry assigned to the calix[4]pyrrole core of the four cavitands, the energy minimized structure always converged to a cone conformation. In short, it was not possible to energy minimize any of these cavitands with the calix[4]pyrrole core exhibiting 1,2- or 1,3-alternate conformations. The energy minimized models showed that the four phenyl bridging groups attached at the upper rims of **8** and **10**, the diazanaphthalenes of **12** and the four 1,3-pyrazine units in **14** resemble flaps that can adopt axial (a) or equatorial (e) orientations. Consequently and in close analogy to the cavitands derived from resorcin[4]arene **1**,²⁹ we expected that cavitands **8**, **10**, **12** and **14** could also adopt kite and vase conformations. The structures of the new cavitands in both conformations were energy minimized using MM3 (see Figure 4 for cavitand **10** including one molecule of DMF).

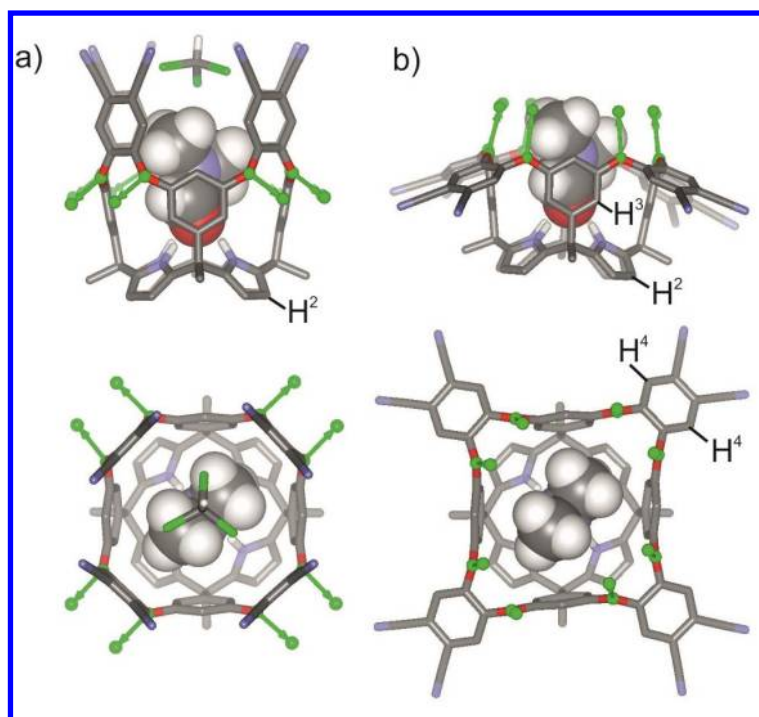


Figure 4. Side and top views of the MM3 energy minimized structures of: a) vase (a,a,a,a) conformer of cavitand **10** modeled with one molecule of DMF (shown as CPK model) and one molecule of

chloroform (stick representation) included in its cavity, and b) kite (e,e,e,e) conformer with C_{4v} -like symmetry. Non-polar hydrogen atoms are omitted for clarity. The kite conformer is modeled with just one molecule of DMF included. The average orientation of the lone-pairs on the oxygen atoms (Lp) in the two structures is indicated by green vectors included in the plane defined by the Lp1-oxygen atom-Lp2 and bisecting the angle they define. Lp = lone-pair electrons of the oxygen atom.

The MM3 energy minimized vase (a,a,a,a) conformer of the calix[4]pyrrole cavitands possess C_{4v} -like symmetry. In this conformation, the fixed aromatic cavity defined by the *meso*-phenyl substituents is significantly increased by the four bridging aromatic panels. For example, in the energy minimized structure of the vase conformer of **10** one molecule of DMF and one molecule of chloroform could be included in its deep aromatic cavity (Figure 4a). The MM3 energy minimized kite structures of the cavitands also displayed C_{4v} -like symmetry. As shown for the kite conformer of **10** (Figure 4b) the lone pairs of the eight oxygen atoms are outwardly directed with respect to its fixed aromatic cavity. Using the MM3 force-field as implemented in the Scigress Program,³⁰ the energy difference for the two conformers of **10** containing one DMF molecule included in their aromatic cavity is 12.7 kcal/mol more favorable as the kite.

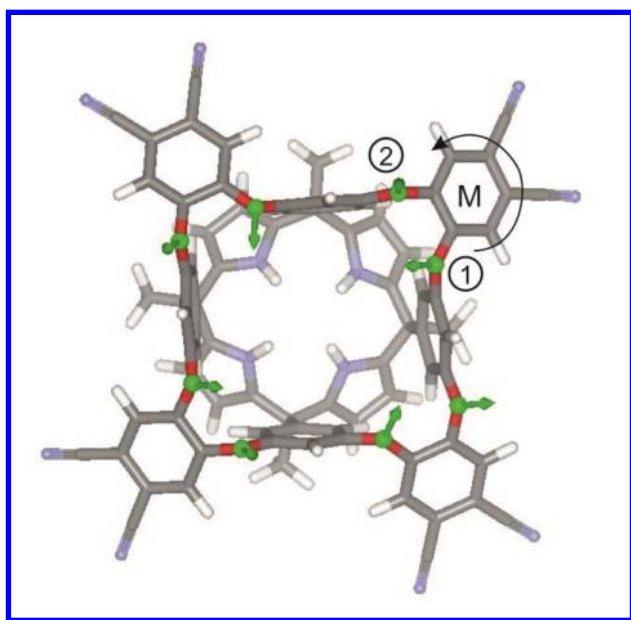


Figure 5. Energy minimized structure of the kite conformer of **10** displaying C_4 symmetry at the BP86-D3/def2-SVP level of theory.

We computed the energy difference between the empty vase and kite conformers of **10** at the BP86^{31,32}-D3³³/def2-SVP level of theory using TURBOMOLE version 6.4.³⁴ C_4 symmetry restrictions were imposed to both structures in order to speed up the calculation time. Interestingly, the energy minimized kite conformer of **10** with C_4 symmetry featured the lone pairs of four of the eight oxygen atoms inwardly directed with respect to the aromatic cavity representing an example of an inherently chiral concave molecule (Figure 5).³⁵ The cyclochiral conformer shown in Figure 5 is defined to have *M* axial chirality assuming that the oxygen atom with the inwardly directed lone pair takes priority over the one having outwardly directed lone pairs.^{36,37} This structure is reminiscent to the kite conformation of resorcinarene cavitands, however in this latter case they exhibited C_{2v} symmetry.^{1,2} At this level of theory, the energy difference between the inclusion complexes of 4-phenyl-pyridine-*N*-oxide **17** with the vase and kite conformers of **10** is 8 kcal/mol in favor of the kite (see SI). Taken in concert, the results of the theoretical calculations indicated that cavitand **10** should adopt exclusively the kite conformation, either displaying C_{4v} or C_4 symmetry. A reverse trend of energies was computed for the two forms of the inclusion complex of the same *N*-oxide and the pyrazine-based cavitand **17**⊂**14** (ΔE = 8.8 kcal/mol in favor of the vase) (SI). Moreover, diazanaphthalene cavitand **12** shows a significant energy preference for the vase form of the inclusion complex with phenyl pyridine *N*-oxide, **17**⊂**12** (ΔE = 22 kcal/mol in favor of the vase) (SI).

The ¹H NMR spectra of the deep cavitands **10**, **12** and **14** taken in different solvents (CD₂Cl₂, toluene-*d*₈) and at different temperatures (-60 °C to 100 °C) show sharp proton signals, the number of which is consistent with a C_{4v} symmetry. The signals do not experience substantial changes in their chemical shifts and shapes as the temperature is changed. At room temperature and in CDCl₃ solutions the β-pyrrolic protons (H²) of the aromatic bridged cavitands resonate at $\delta \sim 5.7$ ppm (see Scheme 2 and Figure 4 for proton assignment). Thus, they appear upfield ($\Delta\delta = -0.32$ ppm) from the β-pyrrolic protons (H²) of the conformationally rigid methylene bridged cavitand **15** (Figure 6) that resonate at $\delta = 6.02$ ppm. In addition, the doublet of the H³ protons in the resorcinol units of the aryl bridged cavitands

($\delta = 5.84, 5.87, 5.76$, and 5.54 ppm for **8**, **10**, **12** and **14** respectively) are also shifted upfield ($\Delta\delta \sim -0.4$ - 0.7 ppm) with respect to the same signal in **15** ($\delta = 6.3$ ppm). In short, the β -pyrrolic protons H^2 and the aromatic protons H^3 in cavitands **8**, **10**, **12**, and **14** must be close to the shielding cone exerted by the bridging aromatic ring. In sum, these NMR observations suggest that in solution and in the range of studied temperatures the aromatic bridged cavitands are locked in the kite (e,e,e,e) conformation. A result that is in not in agreement with the theoretical calculations discussed above.

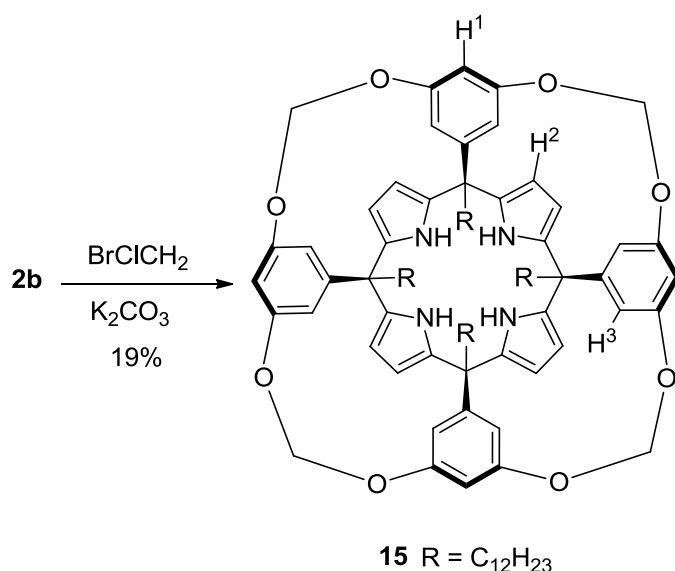


Figure 6. Synthetic scheme of the methylene bridged cavitand **15**.

Moreover, a kite conformer displaying C_{4v} symmetry would explain the reduced number of proton signals observed in the 1H NMR spectra. However, the putative existence of a chemical exchange process (cycloenantiomerization) between two cyclochiral C_4 kite conformers that is fast on the 1H NMR chemical shift time scale at any of the investigated temperatures (213-378 K) could also explain the absence of signal splitting for diastereotopic protons, i.e. H^4 and $H^{4'}$, which can be expected for a kite structure with C_4 symmetry (Figure 7).

Luckily, single crystals of cavitands **8**, **10** and **12** suitable for X-ray diffraction analysis grew from separate solutions of acetonitrile or acetonitrile/dichloromethane mixtures. In the three cases, the cavitands, in the solid state, adopted a kite conformation with C_4 symmetry having one molecule of

solvent included in their fixed aromatic cavities: DMF for **10** and CH₃CN for **8** and **12**. The solvent molecule is hydrogen bonded simultaneously to the four pyrrole N-H hydrogen atoms and the calix[4]pyrrole core adopts a cone conformation (Figure 7).

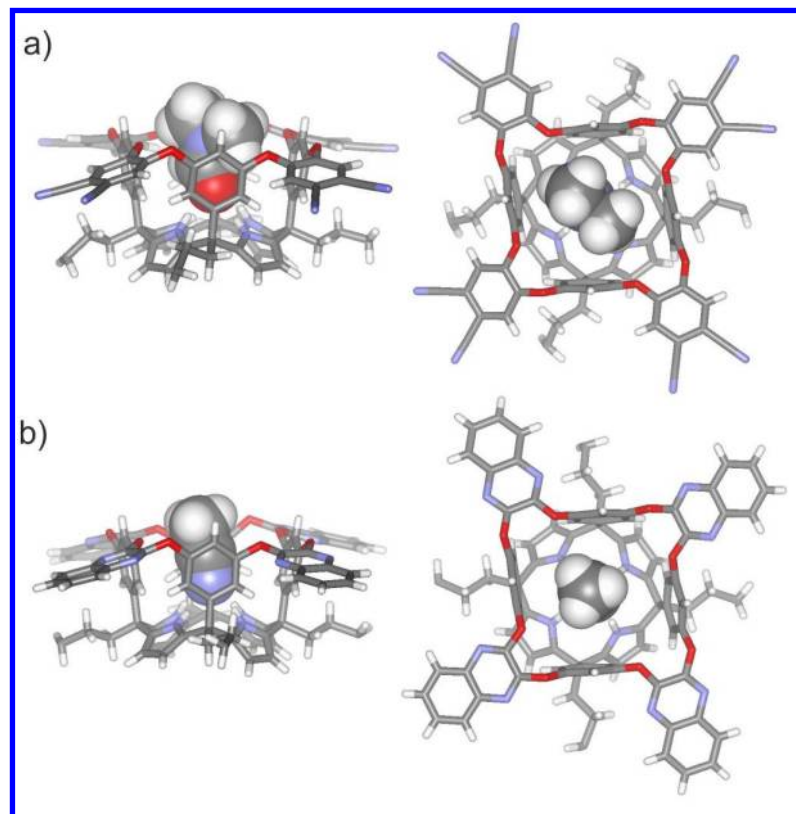
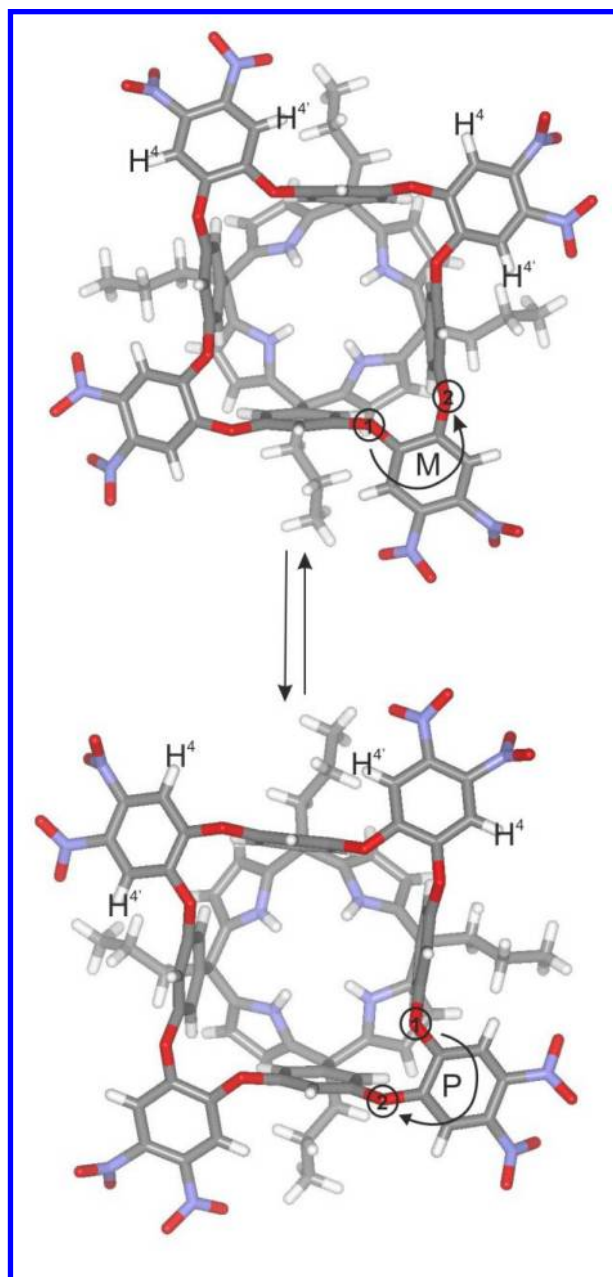


Figure 7. Side and top views of the X-ray structures of the C_4 kite conformer of cavitands: a) DMF \subset **10** and b) CH₃CN \subset **12**. Only the *M* cyclochiral conformer is shown and the length of the *meso*-alkyl groups is truncated to three methylenes for clarity. The cavitands are displayed in stick representation and the included solvent molecules are shown as CPK models.

For the three different cavitands, as could be expected, the two cyclochiral (*M* and *P*) enantiomers of the C_4 kite conformer are present in the packing of the lattice. Most likely, in solution the kite structures of the cavitands are also C_4 symmetric but the two cyclochiral conformers are rapidly interconverting on the ¹H NMR timescale (Scheme 3).



Scheme 3. Cycloenantomerization equilibrium between the two cyclochiral *M* and *P* kite *C*₄ conformers of **8**. The structures of the two cyclochiral enantiomers were extracted from the packing of the X-ray structure of the crystal. The *meso*-alkyl groups are truncated to three carbons for clarity. In solution the interconversion process is fast on the ¹H NMR chemical shift timescale and the diastereotopic protons H⁴ and H^{4'} resonate as one signal even at temperatures below 220 K.

The structure of the transition state for the cycloenantomerization process was investigated by means of theoretical calculations at the BP86-D3/def2-SVP level of theory for the interconversion between the cyclochiral conformers of the octacyano cavitand **10** (see SI). The energy of the transition state lies just

0.9 kcal/mol higher than the C_4 kite ground state of the cyclochiral conformers. The structure of the transition state is similar to that of a kite conformer with C_{4v} symmetry obtained in the energy minimization runs using MM3 (Figure 4b and SI). The low energy barrier computed for the transition state suggests that it is not possible to induce a slow exchange interconversion process on the NMR timescale by lowering the temperature. Consequently, in agreement with experiment, the diastereotopic protons H^4 and $H^{4'}$ (see Scheme 2 and Scheme 3 for proton assignment) of the C_4 kite conformers are observed as one signal.

Molecular recognition studies of pyridine *N*-oxides derivatives by calix[4]pyrrole based deep cavitands. Attempts to change the relative thermodynamic stabilities of the vase and kite forms by guest inclusion.

Pyridine *N*-oxides are important targets for molecular recognition studies due to their pronounced biological activity.^{38,39} We reported that aryl extended calix[4]pyrroles⁴⁰ and their supramolecular capsular derivatives^{41,42,43} bind pyridine *N*-oxides and other aromatic and aliphatic *N*-oxides with high affinity. The oxygen atom of the *N*-oxide forms four simultaneous hydrogen bonds with the pyrrole NHs of the calix[4]pyrrole core. The *N*-oxide guests are bound deep in the aromatic cavity of the host and experience additional CH- π and π - π intermolecular interactions with the *meso*-aryl substituents. Based on our previous findings, we decided to investigate the interaction of the calix[4]pyrrole deep cavitands synthesized in this work with a series of pyridine *N*-oxides (Figure 8).

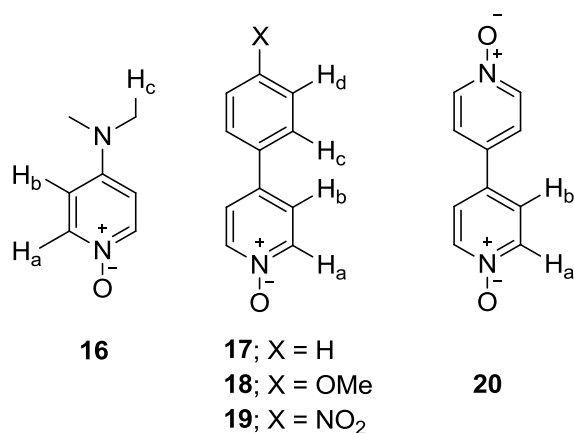


Figure 8. Molecular structures of the pyridine *N*-oxide derivatives used in this work

We first probed the binding of the *N*-oxides by these cavitands in CDCl₃ solution using ¹H NMR spectroscopy. The addition of 0.5 equivalents of 4-dimethylaminopyridine *N*-oxide **16** to a 1 mM CDCl₃ solution of octanitro cavitand **8** resulted in two sets of signals of equal intensity for the protons of the host (Figure 9). The two sets of signals belong to the protons of free and bound host **8**, indicating that the chemical exchange process is slow on the ¹H NMR timescale. The large downfield shift ($\Delta\delta = 1.29$ ppm) observed for the pyrrole NHs of bound **8** is indicative of the formation of hydrogen bonds with the oxygen atom of the bound *N*-oxide **16**. Protons H², H³ and H⁴ of host **8** experience reduced changes of their chemical shifts with respect to the free state, while H¹ shifts slightly upfield ($\Delta\delta = -0.23$ ppm). This effect is probably due to the shielding effect of the bound *N*-oxide. The signals assigned to the aromatic protons of bound **16** moved upfield (H_a $\Delta\delta = -3.13$ ppm and H_b $\Delta\delta = -0.42$ ppm) supporting the inclusion of the *N*-oxide in the fixed aromatic cavity of **8**. In the presence of 1 equivalent of **16** only the proton signals assigned to the bound host and the bound guest were detected. This observation indicates the quantitative formation of a 1:1 complex, **16**⊂**8**, for which a stability constant value larger than 10⁴ M⁻¹ can be estimated. The addition of an excess of **16** did not induce any change in the chemical shifts of the protons assigned to the 1:1 complex. However, signals for the protons of free **16** became visible in the ¹H NMR spectrum of the mixture. A 2D-EXSY experiment performed on a 1 mM solution of cavitand **8** containing 1.5 equivalent of *N*-oxide **16** revealed the absence of cross peaks between the signals of the free and bound *N*-oxide. This result shows that the exchange rate between the free and bound *N*-oxide is too slow to be measured with this technique and suggest that the **16**⊂**8** complex is kinetically very stable (> 5 s).

It is worth noting that the incremental addition of *N*-oxide **16** to the CDCl₃ solution of **8** induced the emergence and subsequent growth of the proton signals characteristic for DMF. We rationalized this observation assuming that cavitand **8** is isolated as a DMF solvate. The DMF molecule is included in the cavity of **8** and it is bound to the four pyrrole NHs through the oxygen atom (see X-ray structure of **10**

in Figure 10). The included DMF could not be removed even after heating a sample of **8** for 24 h under high vacuum conditions. Most likely, the octanitro cavitand **8** binds *N*-oxide **16** considerably stronger than DMF inducing the exchange of guests and the release of free DMF to the bulk solution. The exchange of a bound DMF molecule by the included *N*-oxide is observed in all titration experiments performed with the cavitand series. The elemental analysis of the yellow solid isolated as cavitand **8** is in agreement with the presence of one molecule of DMF for each cavitand.

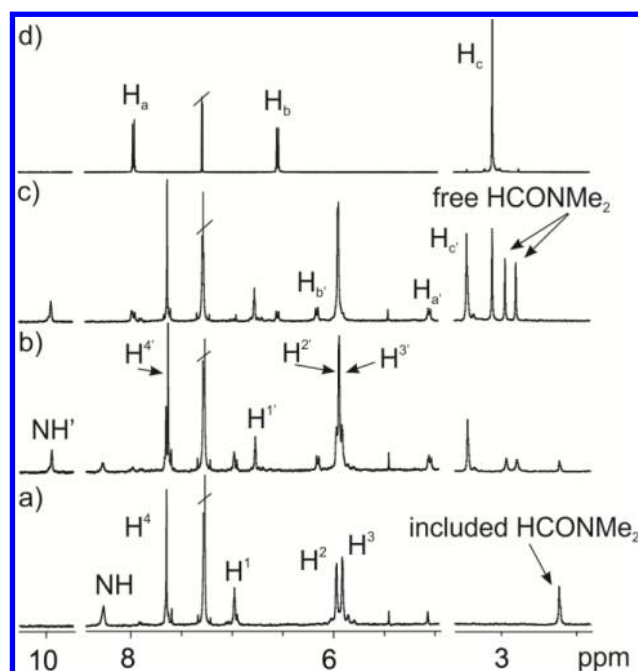


Figure 9. Selected region of ^1H NMR spectra acquired during the titration of a 1 mM CDCl_3 solution of cavitand **8** with incremental amounts of DMAP *N*-oxide **16**: a) 0 eq. b) 0.5 eq. c) 1.5 eq. Panel d) ^1H NMR spectra of free *N*-oxide **16** in CDCl_3 solution. Primed letters and numbers indicate protons in the **16** \subset **8** complex. See Scheme 2 and Figure 8 for proton assignments.

The minimal chemical shift changes observed for the H^2 and H^3 protons of **8** upon binding suggest that in the **16** \subset **8** complex the cavitand maintains the kite conformation. Single crystals of the **16** \subset **8** complex suitable for X-ray diffraction grew from the CDCl_3 solution. The solid state structure of the **16** \subset **8** complex is in complete agreement with that assigned in solution based on the observed chemical shift changes. In the crystal, the bound octanitro cavitand **8** is in the kite form with the calix[4]pyrrole core in the cone conformation displaying an overall C_4 -like symmetry. The oxygen atom of the bound

N-oxide **16** is hydrogen bonded to the four pyrrole NHs. The aromatic protons, alpha to the nitrogen atom, are included in the fixed aromatic cavity of **8**. The pyridyl group of the *N*-oxide experiences simultaneous π - π and CH- π interactions with the *meso*-aryl walls of the cavitand.

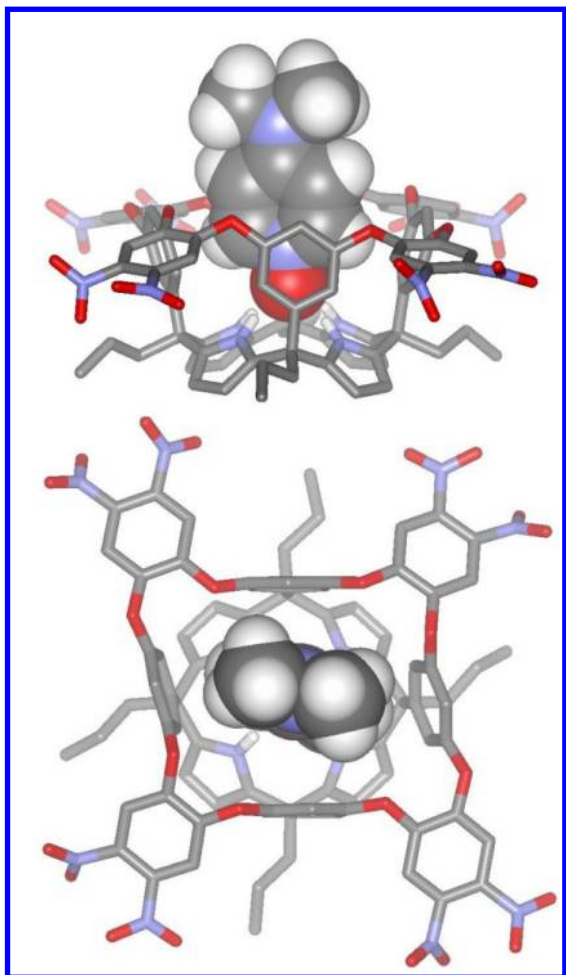


Figure 10. Side and top views of the X-ray structure of the **16**⊂**8** complex. Non polar hydrogen atoms of **8** are removed and alkyl chains are pruned for clarity. *N*-oxide **16** is shown as CPK model and **8** in stick representation.

Completely analogous results were obtained in the titration of octacyano cavitand **10** with 4-dimethylaminopyridine *N*-oxide **16**.

After the addition of 1 equivalent of DMAP *N*-oxide **16** to a 1 mM CDCl₃ solution of cavitand **12**, the formation of a 1:1 inclusion complex was observed in the ¹H NMR spectrum. The large downfield shift of the pyrrolic NHs ($\Delta\delta = 1.59$ ppm) and the upfield shift of the protons for the included guest clearly support the formation of the inclusion complex **16**⊂**12**. In contrast with the titration results obtained for

the previous cavitands, **8** and **10**, the formation of the 1:1 inclusion complex between the DMAP *N*-oxide **16** and the tetradiazanaphthalene cavitand **12** generated a reduced upfield shift for the H¹ proton ($\Delta\delta = -0.08$ ppm for **16**⊂**12** vs -0.23 ppm **16**⊂**8** and **16**⊂**10**). Concomitantly, the H³ proton of bound cavitand **12** moved downfield ($\Delta\delta = 0.15$ ppm). The chemical shift of the H³ proton in cavitands **8** and **10** was almost unaffected upon *N*-oxide binding. These unparalleled chemical shift changes observed for the H¹ and H³ protons in the titration of tetradiazanaphthalene cavitand **12** with **16** suggested to us the possible existence of a conformational switch of the diazanaphthalene flaps, from the axial to equatorial position, induced by the binding of the *N*-oxide. That is, the **16**⊂**12** complex could exist in solution as an undetermined mixture of vase and kite forms of the cavitand involved in a fast chemical exchange on the ¹H NMR timescale.

To further explore the putative complexation induced conformational switch of **12**, we decided to use 4-phenylpyridine-*N*-oxide **17** as a guest. Our expectations were that the *para*-phenyl substituent of *N*-oxide **17** should favor the formation of the **17**⊂**12** complex in vase form. On the one hand, the phenyl substituent is shape and size complementary to the additional aromatic cavity present in the vase conformer of **12** compared to the kite. Additionally, the vase conformer of complex **17**⊂**12** should be energetically favored by additional π - π and CH- π interactions established between the *para*-phenyl substituent of **17** and the diazanaphthalene flaps in the axial conformation (Figure 11). As expected, the interaction of phenyl *N*-oxide **17** with cavitand **12** featured a slow chemical exchange process on the ¹H NMR timescale. The ¹H NMR analysis of an equimolar mixture of **17** and **12** in CDCl₃ solution revealed the quantitative formation of the **17**⊂**12** complex. Unexpectedly, the magnitude of the downfield shift experienced by the H³ proton in the **17**⊂**12** complex ($\Delta\delta = 0.15$ ppm) was coincident with the one observed for inclusion of the shorter *N*-oxide **16**. This result constituted an indication of the failure to provoke a notable guest-induced switch of the kite to the vase form in the inclusion complex **17**⊂**12**.

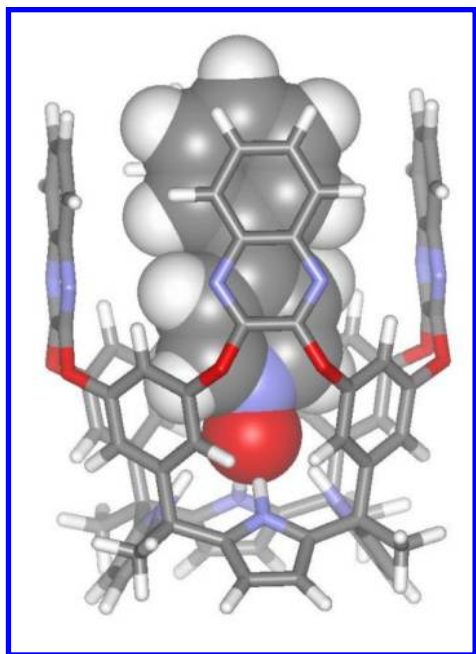


Figure 11. MM3 energy minimized structure of the putative **17**⊂**12** complex in the vase form.

In addition, the signals of the protons pertaining to the *para*-phenyl substituent of included **17** did not shift noticeably with respect to those of the free *N*-oxide. To evaluate if the modification of the electronic properties of the *p*-phenyl ring of the pyridine *N*-oxide had any effect on the possible conformational switch of the bound cavitand **12**, we prepared 4-(4-methoxyphenyl)pyridine *N*-oxide **18** and 4-(4-nitrophenyl)pyridine *N*-oxide **19** (Figure 8). Both pyridine *N*-oxide derivatives produced 1:1 complexes with **12**. The stability constant values for these complexes can be estimated to be larger than 10^4 M^{-1} in CDCl_3 solution. In the case of the methoxy-*N*-oxide **18**, the signal of the H^3 proton of **12** in the inclusion complex **18**⊂**12** shifts upfield 0.14 ppm, a value that coincides with the one observed for the **17**⊂**12** complex. Interestingly, the upfield shift experienced by the H^3 proton in the **19**⊂**12** complex with the nitro *N*-oxide is larger, 0.21 ppm. Additionally, the signal of the *ortho* protons of the *p*-nitrophenyl ring of **19** in the latter complex move somewhat upfield ($\Delta\delta = -0.23 \text{ ppm}$). Taken together, these results suggest, that in solution, the nitro *N*-oxide **19** is capable of inducing a kite to vase conformational switch of the bound cavitand **12** in a larger, although undetermined, extent than the other pyridine *N*-oxide derivatives **17** and **18**. In contrast with these findings, the analysis of the X-ray diffraction data of single crystals of complexes **17**⊂**12**, **18**⊂**12** and **19**⊂**12** revealed that, in the solid

1 state, cavitand **12** exclusively adopts the kite form in the three inclusion complexes (Supporting
2 Information).

3
4
5 Pyridine *N*-oxides **18** and **19** were also used to investigate the putative guest induced conformational
6
7 switch using the shorter aryl bridged cavitands **10** and **14**. The obtained results point to exclusive
8
9 formation of inclusion complexes in which the shorter cavitands are in the kite form (Supporting
10
11 Information).

12
13
14 Tetramethylene bridged cavitand **15** is deprived of aromatic flaps and constitutes an ideal reference to
15
16 determine the expected chemical shift changes for the protons of the host induced by the inclusion of *N*-
17
18 oxides. The equimolar mixture of methylene bridged cavitand **15** and 4-phenylpyridine *N*-oxide **17** in
19
20 CDCl₃ solution at 1 mM concentration produced the quantitative formation of the **17**⊂**15** complex. The
21
22 ¹H NMR spectrum of the mixture indicated that, in response to guest inclusion, the H¹ proton in **15**
23
24 moves upfield ($\Delta\delta = -0.53$ ppm). Most likely, the observed chemical shift change is due to the shielding
25
26 effect produced by the *para*-phenyl group of the included *N*-oxide. In addition, the chemical shift values
27
28 of protons H² and H³ in **15** are insensitive to the inclusion process. These results provide strong support
29
30 to the hypothesis that the detected changes in chemical shifts for equivalent protons in cavitand **12** are
31
32 indeed caused by a conformational change in the aromatic flaps.
33
34
35
36
37

38 We wanted to evaluate the effect of temperature in the kite to vase conversion of cavitand **12** when
39
40 involved in the formation of inclusion complexes with *N*-oxides. It is known that in related cavitands
41
42 derived from a resocin[4]arene scaffold, the vase form is favored at high temperatures owed to an
43
44 increase in the negative entropic term over the positive enthalpy component of the kite to vase
45
46 conversion.⁴⁴ The variable temperature experiments were performed in solutions of tetrachloroethane-
47
48 *d*₂, a solvent with a boiling point of 146 °C. In this solvent and at 298 K, the chemical shift changes
49
50 experienced by the protons of the complexes between cavitand **12** and the series of pyridine *N*-oxides
51
52 **17**, **18** and **19** were similar to those observed in CDCl₃ solution.
53
54
55
56

57 Increasing the temperature to 398 K amplifies the chemical shift changes. For the three inclusion
58
59 complexes, the downfield shift experienced by H³ in bound **12** increases two-fold. Similarly, the upfield
60

1 shift of the *ortho*-proton, H_c, in the phenyl substituent of the included *N*-oxides doubles its magnitude.
2
3 Taken in concert, these data suggest that the increase in temperature favors the vase form of the cavitand
4
5 **12** in the inclusion complexes. Unfortunately, the available data do not allow the determination of an
6
7 accurate percentage of kite and vase forms of the cavitand in these complexes at different temperatures.
8
9

10 Similar variable temperature experiments performed with an equimolar mixture of the shorter
11
12 tetrapyrazine cavitand **14** and methoxyphenyl *N*-oxide **18**, revealed that in the **18**⊂**14** complex the
13
14 chemical shifts of protons H³ and H_c are not modified by temperature changes. This result underlines a
15
16 clear conformational preference for the kite form in bound cavitand **14**. This is in contrast with the
17
18 observations made with related pyrazine cavitands based on resocin[4]arene scaffolds, which are locked
19
20 in the vase form.²
21
22
23

24 From the results obtained in the ¹H NMR titration experiments, the stability constants of the 1:1
25
26 inclusion complexes formed between cavitands, **8**, **10**, **12** and **14**, and pyridine *N*-oxide derivatives, **16**,
27
28 **17**, **18**, **19** and **20**, were estimated to be larger than 10⁴ M⁻¹ (quantitative formation of the 1:1 complex in
29
30 the presence of equimolar amounts of host and guest at mM concentration). For this reason, we
31
32 undertook the calculation of accurate values for the stability constants of these 1:1 complexes using
33
34 isothermal titration calorimetry (ITC) experiments. The ITC data obtained for the titrations of
35
36 designated cavitands (**12** and **10**) with phenyl pyridine *N*-oxide **17** pictured double sigmoid curves.
37
38 Figure 12 displays the plot of the normalized integrated heat (black diamonds) vs molar ratio [17]/[12]
39
40
41 for the titration of **12** with phenyl-*N*-oxide **17**.
42
43
44
45
46
47
48
49
50
51
52
53
54
55
56
57
58
59
60

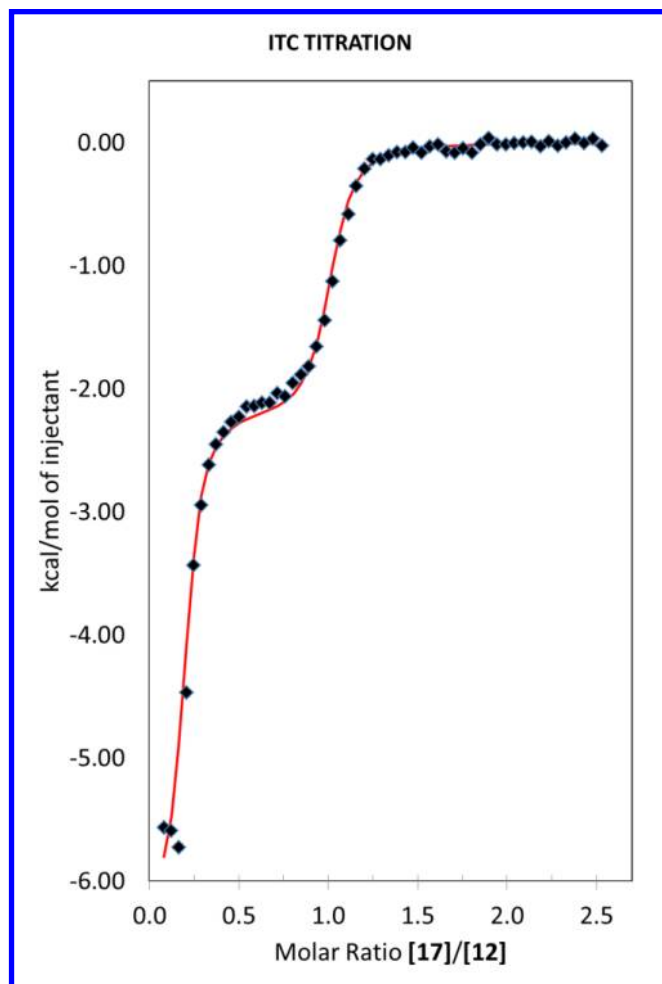


Figure 12. Plot of the normalized integration heat (black diamonds) vs $[17]/[12]$ molar ratio obtained for the ITC experiment of **12** (0.99 mM) with **17** (9.8 mM) in CHCl_3 . Theoretical binding isotherm (red line) for a binding model that considers three species, **12**, DMF, **17**, and two complexes $\text{DMF} \subset \text{12}$ and $\text{17} \subset \text{12}$, fit to the experimental data is also shown.

The two inflexion points of the double sigmoid binding isotherm are centered at values close to 0.25 and 1 for the molar ratio $[17]/[12]$. ITC dilution experiments performed on both the cavitand and the pyridine *N*-oxide showed insignificant release of heat. In addition, a DOSY NMR experiment carried out with a CDCl_3 solution containing a 2:1 mixture of cavitand **12** and phenyl *N*-oxide **17** provided similar diffusion coefficient values for the free and bound cavitand. These findings ruled out the existence of dimerization/oligomerization processes for **12** or **17** in solution in the range of used concentrations. As we already commented above, the solid isolated as cavitand **12** was in fact, to a great extent, a DMF solvate of **12**. Based on this precedent and using the HypDH software, we were able to fit

the double sigmoid binding curve to a theoretical binding model that considers the existence of three species and five stoichiometric states: free **12**, free DMF, free **17**, DMF \subset **12** and **17** \subset **12** (Figure 12). The concentration of DMF in the calorimetric cell was determined to be $0.85 \times [\mathbf{12}]$.⁴⁵ In short, only 15% of the molecules in the solid isolated as **12** do not include a molecule of DMF. The fit of the ITC data returned the values of $\Delta H(\text{DMF} \subset \mathbf{12}) = -4.1$ kcal/mol, $\Delta H(\mathbf{17} \subset \mathbf{12}) = -6.3$ kcal/mol, $K(\text{DMF} \subset \mathbf{12}) = 5.5 \times 10^5 \text{ M}^{-1}$ and $K(\mathbf{17} \subset \mathbf{12}) = 6.3 \times 10^7 \text{ M}^{-1}$. The two orders of magnitude difference measured for the stability constants of the complexes of **12** indicates the almost exclusive formation of the **17** \subset **12** complex when DMF and *N*-oxide **17** are in solution in an equimolar ratio with respect to **12**. The speciation profiles derived from the ITC experiments are in complete agreement with the observations made in the ¹H NMR titrations of **12** with **17** (release of approximately one equivalent of DMF to the bulk solution on addition of one equivalent of **17**). We attempted to remove the DMF from the solid isolated as cavitand **12** by continuous heating under high vacuum. However, the ITC experiments performed with samples of **12** treated as indicated above also produced double-sigmoid binding curves with reduced changes in the molar ratio of the first inflexion point. The deep inclusion of DMF in the conformationally rigid aromatic cavity of **12** means that its release is energetically highly disfavored because it produces an empty cavity (vacuum). The deep inclusion nature of complexes **17** \subset **12** and DMF \subset **12** is also responsible of the favorable entropic terms (3.3 kcal/mol and 3.7 kcal/mol, respectively) determined for their complexation processes. Both host and guest must experience strong desolvation processes prior to the formation of the inclusion complex. The release of solvating chloroform molecules to the bulk solution assists binding entropically, even in such a non-polar solvent, overcoming the loss of translational and rotational entropy of one of the partners and of the conformational flexibility of host and guest bound in the complex.

We decided to grade the stability constant values of some inclusion complexes of cavitands **12** and **10** with designated phenyl-*N*-oxides by performing pairwise competitive experiments and analyzing them using ¹H NMR spectroscopy. An equimolar mixture of cavitand **12** with phenyl-*N*-oxide **17** and

methoxyphenyl-*N*-oxide **18** in CDCl₃ produced inclusion complexes **17**⊂**12** and **18**⊂**12** in an exact 1:1 ratio, demonstrating that the stability constant values of the two complexes are independent of the electronic nature of the *para*-phenyl substituent of the *N*-oxide. We also performed a pairwise competitive experiment by mixing equimolar amounts of cavitands **10** and **12** with methoxyphenyl- *N*-oxide **18**. The obtained CDCl₃ solution was analyzed by ¹H NMR spectroscopy indicating the formation of complexes **18**⊂**10** and **18**⊂**12** in equal amounts. This latter result proves that the stability constants of the caviplexes resulting from calix[4]pyrrole cavitands **10** and **12** and pyridine *N*-oxides are not significantly influenced by the characteristics of the bridging aromatic ring.

The preference exhibited by cavitand **12** to adopt the kite form in the inclusion complexes with pyridine *N*-oxides prompted us to investigate the formation of three-component aggregates involving one molecule of a bis-*N*-oxide (ditopic guest) and two units of cavitand **12**. Molecular modelling studies indicate that 4,4'-dipyridyl-*N,N'*-dioxide **20** is a suitable molecular platform to study such assembly process. The energy minimized structure of the complex **20**⊂**12**₂ did not show clear signs of attractive or repulsion interactions between the two units of **12** (Figure 13).

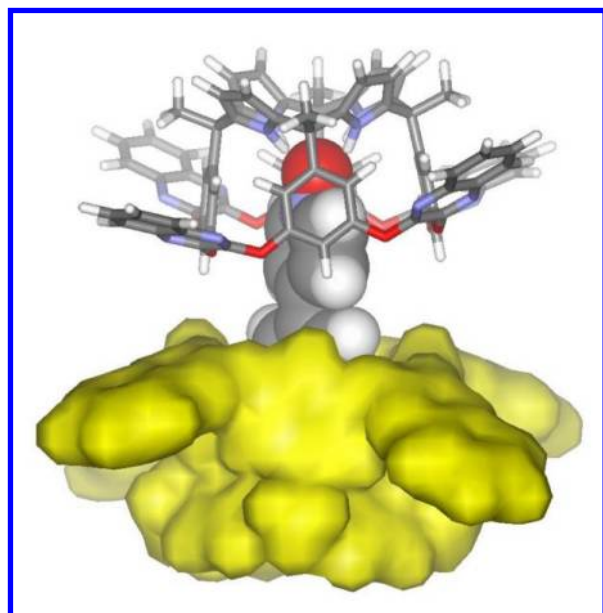


Figure 13. Energy minimized structure of the **20**⊂**12**₂ complex. One unit of **12** is depicted in stick representation, the other as van der Waals surface and the bis-*N*-oxide **20** is shown as CPK model.

The binding of bis-*N*-oxide **20** with **12** was probed in CDCl₃ solution using ¹H NMR spectroscopy. Addition of 0.25 equivalents of bis-*N*-oxide **20** resulted in the appearance of a new set of signals (Figure 14b). We assigned the new signals to the protons of the cavitand **12** in the **20**⊂**12**₂ complex. The pyrrole NHs of the cavitand in the 1:2 complex resonate downfield at δ = 9.27 ppm indicating the formation of hydrogen bonds with the oxygen atom of bound **20**. The protons of bound **20** appear highly upfield shifted: i.e. δ = 5.82 ppm and 7.68 ppm for H_a'' and H_b'', respectively and as unique set. These observations are in agreement with the inclusion of each binding site of **20** in one unit of **12** producing a 1:2 complex, **20**⊂**12**₂, featuring D_{4h}-like symmetry.

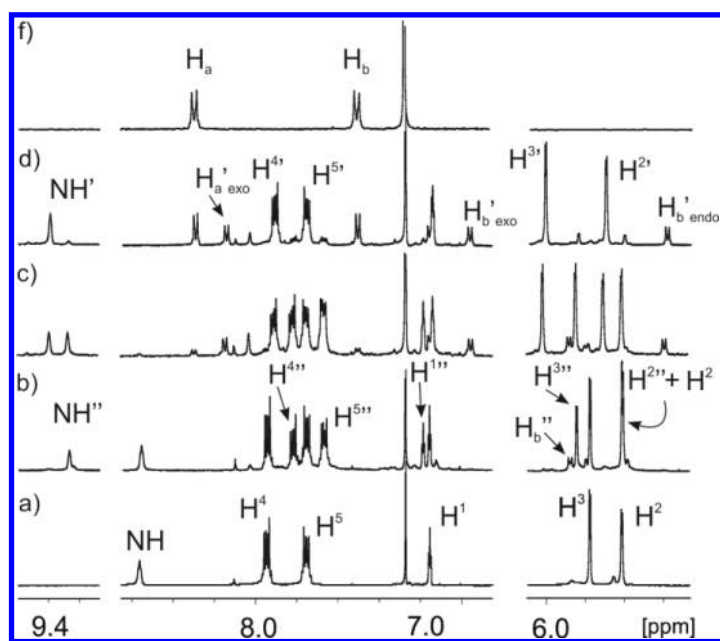
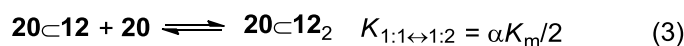


Figure 14. Selected regions of the ¹H NMR spectra acquired during the titration of a 1 mM CDCl₃ solution of tetradiazanaphthalene cavitand **12** with bis *N*-oxide **20**. Equivalents added: a) 0 b) 0.25 c) 0.75 d) 1.5. Panel f) corresponds to the same regions of the ¹H NMR spectrum of **20**. Primed letters and numbers indicate protons in the **20**⊂**12** complex and doubly primed for the **20**⊂**12**₂ complex.

In the presence of 0.5 equivalents of bis-*N*-oxide **20** we observed the emergence of a new set of proton signals for **12** that do not correspond with those assigned to the free host or the 1:2 complex. These signals must correspond to a new inclusion complex in which the pyrrole NHs resonate at δ = 9.40 ppm. Upon further addition of **20**, the intensity of the signals of the latter complex grew at the

expenses of those of **20**⊂**12**₂ (Figure 14c,d). Interestingly, the protons of bound **20** in the new complex resonate as four separate signals. Two of them appear at chemical shift values that are in line with those observed for the included *N*-oxide in the **20**⊂**12**₂ complex. The other two, however, are just slightly upfield shifted with respect to the protons in free **20**. The relative integrals for these four signals are 1:1:1:1. When 0.75 equivalents of **20** are added the signals for the protons of free *N*-oxide start to arise. In the presence of 1.5 equivalents of **20** the **20**⊂**12** complex is the major species in solution. Taken together, these observations indicate that the incremental addition of **20** induces the destruction of the **20**⊂**12**₂ complex and induces the formation of a new 1:1 complex, **20**⊂**12**. The observation of four proton signals for the included *N*-oxide in the **20**⊂**12** complex is consistent with its lower symmetry. The determination of accurate values for the stability constants of the 1:1 complex from the ¹H NMR titration data is hampered by the large value of the microscopic binding constants ($K_m > 10^4 \text{ M}^{-1}$) assigned to the interaction of the pyridine *N*-oxide group with the cavitand **12**. Nevertheless, after all the free cavitand is consumed, it is possible to determine an average value for the equilibrium constant of the destruction process K_d (equation 1) by integrating the signals assigned to the **20**⊂**12** and **20**⊂**12**₂ complexes in the presence of different amounts of **20**.



$$K_d = \frac{K_{1:1}}{K_{1:1 \leftrightarrow 1:2}} = 4/\alpha \quad (4)$$

Scheme 4. Equilibria involved in the destruction of the **20**⊂**12**₂ complex (1) and in the formation of the **20**⊂**12** (2) and **20**⊂**12**₂ (3) complexes. The relationship of the equilibrium constants with K_m (microscopic constant), α (the cooperativity factor), and statistical correction factors are shown.

Using the relationship that exists between K_d and the cooperativity factor (α) of the *N*-oxide **20** (Equation 3 in Scheme 4) we determined α to be 0.09. A value of $\alpha < 1$ for **20** indicates the existence of

a negative cooperativity in the assembly process of the **20**⊂**12**₂ complex. In other words, the second binding event (3) leading to the formation of the **20**⊂**12**₂ complex from the preformed **20**⊂**12** is less favorable than the statistical estimate derived from the microscopic constant value of the first binding event. Most likely, the binding of the second unit of **12** is disfavored by a combination of electrostatic and steric effects. On one hand, the upfield shift observed for the protons of the diazanaphthalene flaps in the **20**⊂**12**₂ complex suggest their involvement in π - π stacking interactions between adjacent units of **12**. On the other hand, the reduced downfield shift experienced by the pyrrole NHs in the **20**⊂**12**₂ complex compared to those in **20**⊂**12** points to the formation of larger hydrogen bonds in the latter. This can be either a consequence of repulsive interactions between the two units of **12** in the **20**⊂**12**₂ complex or to a modification of negative density of the free oxygen atom of the *N*-oxide in the **20**⊂**12** complex. The existence of a negative cooperativity in the assembly of the **20**⊂**12**₂ complex is also supported by the observation of a solution mixture of free **12**, **1:1** and **1:2** complexes when working under strict stoichiometric control (ratio of [**20**]/[**12**] = 0.5).

CONCLUSIONS

We report here the synthesis of a novel family of deep-cavitands based on a calix[4]pyrrole scaffold. The cavitands have been characterized both in the solid state and in solution. Whereas resorcinarene-based cavitands easily switch between the vase and the kite conformations with temperature, the calix[4]pyrrole-derived cavitands are conformationally more rigid than their resorcinarene analogs. In the range of conditions studied they are locked in a *C*₄ kite form as a racemic mixture of two cycloenantiomers. Molecular modeling studies are in agreement with the experimental observations. The energy barrier calculated for the interconversion between cycloenantiomers is very low (0.9 kcal/mol) explaining the fast interconversion observed in solution. Pyridine *N*-oxide derivatives are included by the deep cavitands yielding 1:1 caviplxes that are thermodynamically and kinetically highly stable. The putative conformational switch between the kite and vase forms of the calix[4]pyrrole cavitands was studied using variable temperatures ¹H NMR experiments and by including *N*-oxide

1 guests that are size and shape complementary to the vase form. The obtained results suggest that only
2 the cavitand decorated with four diazanaphthalene flaps undergoes such conformational switching when
3 the cavitand decorated with four diazanaphthalene flaps undergoes such conformational switching when
4 complexed with an electron-poor pyridine *N*-oxides derivative and at elevated temperature. The extent
5 of the conformational switch could not be determined but the magnitude of the observed chemical shift
6 changes suggest that it is reduced. Finally, the complexation of the ditopic bipyridine bis-*N*-oxide **20**
7 with cavitand **12** produced the formation of the 1:2 complex through a non-cooperative binding process.
8
9

10 Experimental section

11
12
13
14
15
16
17
18 **Methods and materials.** ¹H-NMR and ¹³C NMR spectra were recorded on a 400 and 500 MHz
19 spectrometer. All solvents were dried prior to use. 1,2-difluoro-4,5-dinitrobenzene was prepared
20 according to a reported procedure.⁴⁶ 4,5-difluorophthalonitrile and 2,3-dichloroquinoxaline were
21 commercially available and used without further purification.
22
23
24
25
26

27 **Synthesis of 4.** To an oven-dried 100-mL round-bottomed flask containing magnesium turnings (1.46 g,
28 60 mmol) dry ether (15 mL) was added under argon atmosphere. Bromododecane (7.5 mL, 30 mmol)
29 was added dropwise through a dropping funnel over 30 min under reflux. From the last addition, the
30 reaction was kept under reflux for further 45 min, then a solution of 3,5-dimethoxybenzaldehyde (5 g,
31 30 mmol) in dry ether (25 mL) was added dropwise and the mixture was left reacting for three
32 additional hours. The reaction was quenched by addition of a saturated solution of NH₄Cl (35 mL). The
33 collected organic layers were washed with water, brine and dried over sodium sulphate. The solvent was
34 removed under reduced pressure affording 9.5 g (95% yield) of a white solid that was used without
35 further purification. ¹H NMR (400MHz, CDCl₃): δ= 6.50 (d, J = 2.3 Hz, 2H), 6.37 (t, J = 2.3 Hz, 1H),
36 3.79 (s, 6H), 2.93 (t, J = 7.6 Hz, 2H), 1.72 (m, 2H), 1.21-1.33 (m, 18H), 0.87 (t, J = 6.5 Hz, 3H).
37
38
39
40
41
42
43
44
45
46
47
48
49
50
51 HRMS-ESI+ m/e calcd for C₂₁H₃₅O₂ (M-OH)⁺ 319.2637, found 319.2641
52
53

54 **Synthesis of 5.** In a 250-mL round-bottomed flask filled with dry dichloromethane (40 mL), pyridinium
55 chlorochromate (3.84 g, 17.8 mmol), silica (3.84 g) and alcohol **4** (2g, 5.9 mmol) were added in one
56 portion. The reaction mixture was stirred at rt for two hours, then diluted with ether and filtered over a
57
58
59
60

bed of celite (1 cm) and silica (3 cm). The filtrate was concentrated under reduced pressure and the residue was recrystallized from methanol affording 1.5 g (75% yield) of a white crystalline solid. ^1H NMR (500MHz, CDCl_3 , 298K): δ = 7.09 (d, J = 2.4 Hz, 2H), 6.64 (t, J = 2.4 Hz, 1H), 3.84 (s, 6H), 2.91 (t, J = 7.6 Hz, 2H), 1.71 (m, 2H), 1.21-1.39 (m, 18H), 0.87 (t, J = 6.8 Hz, 3H). HRMS-ESI $^+$ m/e calcd for $\text{C}_{21}\text{H}_{35}\text{O}_3$ ($\text{M}+\text{H}$) $^+$ 335.2586, found 335.2585

Synthesis of 6. In a 10-20 mL microwave vial, ketone **5** (1g, 3 mmol) and pyridinium chloride (3.45 g, 30 mmol) were irradiated at 250 $^\circ\text{C}$ for one hour. The residue was partitioned between water and ethyl acetate. The aqueous layer was extracted three times with ethyl acetate. The combined organic layers were dried over sodium sulphate and the solvent was removed under reduced pressure. Recrystallization of the residue afforded 452 mg (49% yield) of **6** as white solid. ^1H NMR (400MHz, CDCl_3 , 298K): δ = 6.99 (d, J = 2.3 Hz, 2H), 6.54 (t, J = 2.3 Hz, 1H), 2.87 (m, 2H), 1.69 (m, 2H), 1.23-1.33 (m, 18H), 0.87 (t, J = 6.7 Hz, 3H). HRMS-ESI $^-$ m/e calcd for $\text{C}_{19}\text{H}_{29}\text{O}_3$ ($\text{M}-\text{H}$) $^-$ 305.2117, found 305.2115

Synthesis of octahydroxy calixpyrrole 2b. To a 100 mL round-bottomed flask containing a solution of pyrrole (0.25 mL, 3.6 mmol) in MeOH (6 mL), methanesulfonic acid (0.24 mL, 10.77 mmol) was added dropwise. The mixture was stirred for 5 minutes, then a solution of ketone **6** (1.1 g, 3.6 mmol) in MeOH (18 mL) was added slowly and the reaction was left at rt overnight protected from light; then, quenched by addition of water (30 mL) and extracted with ethyl acetate (4 x 50 mL). The combined organic layers were dried over sodium sulphate and the solvent was removed under reduce pressure. The mixture crude was purified by chromatography (SiO_2 ; dichloromethane:ethyl acetate from 8:2 to 6:4) affording a brownish solid that was recrystallized from acetonitrile (245 mg, 19 % yield). ^1H -NMR (500 MHz, MeOD, 25 $^\circ\text{C}$): δ (ppm) = 8.89 (bs, 4H), 6.18 (d, J = 2.0 Hz, 8H), 6.15 (t, J = 2.0 Hz, 4H), 5.89 (d, J = 2.4 Hz, 8H), 2.30 (m, 8H), 1.35 (m, 74H), 0.89 (t, J = 7.0 Hz, 12H); ^{13}C NMR (CDCl_3 /100 MHz) δ 157.0, 148.5, 137.2, 108.4, 104.9, 100.6, 40.1, 38.1, 31.8, 30.2, 29.6, 29.55, 29.50, 29.48, 29.2, 25.22, 22.45, 13.21 HRMS-MALDI $^+$ m/z calculated for $\text{C}_{92}\text{H}_{132}\text{N}_4\text{O}_8\text{Na}$ 1443.9942, found 1443.9937 M.p. > 142 $^\circ\text{C}$ (decomp)

Synthesis of octanitrocalix[4]pyrrole 8: A mixture of octahydroxycalix[4]pyrrole (145 mg, 0.102 mmol) and 1,2-difluoro-4,5-dinitrobenzene (91 mg, 0.445 mmol) are placed in an oven-dried Schlenk flask and dried under vacuum for 10 minutes. Dry DMF (15 mL) was added under argon, and while stirring, triethylamine (distilled over calcium hydride, 0.136 mL, 0.972 mmol) is added dropwise. The flask is heated to 85 °C overnight. The reaction is concentrated under reduced pressure and the residue is purified by column chromatography (silica gel, dichloromethane : hexane 6:4) to give product **8** (100 mg, yield 47%) as a yellowish solid that can be recrystallized from acetonitrile. ¹H NMR (CDCl₃/400 MHz) δ 8.33 (bs, 4H), 7.66 (s, 8H), 6.93 (t, J = 2.0Hz, 4H), 5.85 (d, J = 2.2Hz, 8H) 5.79 (d, J = 2.0Hz, 8H), 2.17 (m, 8H), 1.36-1.13 (m, 80H), 0.88 (t, J = 6.2Hz, 12H); ¹³C NMR (CDCl₃/100 MHz) δ 158.2, 153.0, 150.4, 140.2, 135.2, 120.9, 110.9, 110.5, 106.6, 48.9, 32.0, 29.9, 29.8, 29.7, 29.6, 29.5, 29.4, 22.7, 14.1. MS-MALDI- m/e calcd for C₁₁₆H₁₃₂N₁₂O₂₄ 2076.95, found 2076.8. Anal. Calcd for C₁₁₆H₁₃₂N₁₂O₂₄·DMF: C, 66.43; H, 6.51; N, 8.46. Found: C, 66.82; H, 6.28; N, 8.49. M.p. T > 251 °C (decomp).

Synthesis of octanitritrilecalix[4]pyrrole 10: In a sealed tube the octahydroxycalix[4]pyrrole (200 mg, 0.141 mmol) and 4,5-difluorophthalonitrile (99 mg, 0.605 mmol) are dissolved in 5 mL of dry DMF. Triethylamine (distilled over calcium hydride, 0.196 mL, 1.406 mmol) is added, and the tube is heated to 85 °C overnight. The reaction is concentrated under reduced pressure and the residue is purified by column chromatography (silica gel, dichloromethane) and recrystallized from acetonitrile to afford **9** (186 mg, yield 69%) of an off-white solid. ¹H NMR (CDCl₃/500 MHz) δ 8.33 (bs, 4H), 7.52 (s, 8H), 6.93 (t, J = 2.4Hz, 4H), 5.87 (d, J = 2.6Hz, 8H) 5.70 (d, J = 2.4Hz, 8H), 2.17 (m, 8H), 1.37-1.24 (m, 80H), 0.90 (t, J = 6.3Hz, 12H); ¹³C NMR (CDCl₃/100 MHz) δ 158.4, 152.7, 151.2, 135.3, 129.3, 114.2, 113.8, 110.2, 106.2, 105.8, 48.8, 39.3, 37.6, 32.0, 30.0, 29.9, 29.8, 29.7, 29.6, 29.5, 29.4, 25.6, 22.8, 14.2. HRMS-MALDI m/z calculated for C₁₂₄H₁₃₂N₁₂O₈ 1917.0291, found 1917.0286. M.p. T > 292 °C (decomp).

Synthesis of tetraquinoxaline 12: In a sealed tube the octahydroxycalix[4]pyrrole (500 mg, 0.352 mmol), 2,3-dichloroquinoxaline (361 mg, 1.758 mmol) and dry potassium carbonate (486 mg, 3.52 mmol) are placed. 10 mL of dry DMF are added and the tube is heated to 85 °C overnight. HCl 1N (10 mL) was added and the precipitate was filtered under vacuum. Purification of the solid by column chromatography (silica gel, dichloromethane) and recrystallization from acetonitrile afforded **12** as a white solid (345 mg, yield 51%). ¹H NMR (CDCl₃/500 MHz) δ 8.59 (bs, 4H), 7.95 (dd, J₁ = 3.4Hz, J₂ = 6.2Hz, 8H), 7.76 (dd, J₁ = 3.4Hz, J₂ = 6.2Hz 8H), 7.16 (t, J = 2.0Hz, 4H), 5.78 (d, J = 2.0Hz, 8H), 5.61 (d, J = 2.0Hz, 8H), 2.04 (m, 8H), 1.38-1.12 (m, 80H) 0.92 (t, J = 6.1Hz, 12H); ¹³C NMR (CDCl₃/100 MHz) δ 157.7, 150.9, 149.4, 139.7, 135.7, 129.9, 127.9, 111.9, 106.9, 105.2, 48.5, 39.3, 37.8, 31.9, 30.7, 30.2, 30.0, 29.9, 29.9, 29.8, 29.7, 29.4, 24.7, 22.7, 14.1. MS-MALDI+ m/e calcd for C₁₂₄H₁₄₀N₁₂O₈ 1925.1, found 1925.0 Anal Calcd for C₁₂₄H₁₄₀N₁₂O₈·DMF: C, 76.28; H, 7.41; N, 9.11. Found: C, 76.08; H, 7.36; N, 9.14. M.p. T > 328 °C (decomp).

Synthesis of tetrapyrazine cavitand 14: In a sealed tube the octahydroxycalix[4]pyrrole (305 mg, 0.214 mmol), 2,3-dichloropyrazine (118 μL, 1.072 mmol) and dry potassium carbonate (296 mg, 2.145 mmol) are placed; 10 mL of dry DMF are added and the tube is heated to 85 °C overnight, and then, 10 mL of HCl 1N is added and the precipitate is filtered under vacuum. Purification of the solid by column chromatography (silica gel, dichloromethane: THF 98:2) and recrystallization from acetonitrile afforded **14** as a white solid (45 mg, yield 12%). ¹H NMR (CDCl₃/500 MHz) δ 8.19 (bs, 8H), 8.12 (s, 4H), 7.00 (t, J = 2.2Hz, 4H), 5.70 (d, J = 2.5Hz, 8H), 5.54 (d, J = 2.2Hz, 8H), 2.04 (m, 8H), 1.38-1.12 (m, 80H) 0.88 (t, J = 6.5Hz, 12H) ¹³C NMR (CDCl₃/100 MHz) δ 157.9, 150.9, 140.2, 135.7, 111.0, 106.1, 105.2, 48.61, 31.9, 30.0–29.3, 22.7, 14.1. M.p. T > 275 °C (decomp). HRMS-ESI+ m/e calcd for C₁₀₈H₁₃₂N₁₂O₈ (M+Na)⁺ 1748.0189, found 1748.0188.

Synthesis of tetramethylene bridged cavitand 15: In a 25 mL oven-dried Schlenk tube, the octahydroxycalixpyrrole **2b** (21 mg, 0.015 mmol) and oven-dried potassium carbonate (24 mg, 0.174

mmol) were placed and dried under high vacuum for three hours. Then, under argon, 1.2 mL of dry DMF was added. The flask is heated to 85 °C and then, bromochloromethane (50 μ L, 0.769 mmol) is added in just one portion. The flask is heated for an additional three hours. The reaction is concentrated under reduced pressure and purified by column chromatography (silica gel, dichloromethane:hexane 1:1 to pure dichloromethane) to afford the product as a white solid (4 mg, yield 18%). ^1H NMR ($\text{CDCl}_3/500$ MHz) δ 7.46 (bs, 4H), 6.46 (t, J = 2.1Hz, 4H), 6.38 (d, J = 2.1Hz, 8H), 6.10 (d, J = 7.6Hz, 4H), 6.02 (d, J = 2.6Hz, 8H), 5.37 (d, J = 7.6Hz, 4H), 2.35 (m, 8H), 1.38-1.12 (m, 80H), 0.90 (t, J = 6.9Hz, 12H). ^{13}C NMR ($\text{CDCl}_3/100$ MHz) δ 156.6, 149.8, 136.9, 109.1, 108.3, 105.4, 87.9, 48.8, 38.9, 31.9, 30.2, 29.7, 29.6, 29.5, 29.3, 25.1, 22.7, 14.1. HRMS-ESI+ m/e calcd for $\text{C}_{96}\text{H}_{132}\text{N}_4\text{O}_8$ ($\text{M}+\text{Na}$) $^+$ 1491.9943, found 1491.9920.

Synthesis of 4-(4-methoxyphenyl)pyridine *N*-oxide 18: In a 100 mL round bottomed flask, the 4-methoxy(4-phenyl)pyridine (150 mg, 0.810 mmol) is dissolved in 20 mL of dry chloroform. Then, mCPBA is added in small portions (300 mg, 1.215 mmol). After stirring for 2.5 hours at room temperature, an extra portion of mCPBA is added (200 mg). After one hour the reaction is concentrated and eluted through a column of basic alumina, first with dichloromethane and finally with dichloromethane:methanol 9:1 until elution of the pure product as a hygroscopic yellow solid (130 mg, 80% yield). ^1H NMR ($\text{CDCl}_3/500$ MHz) δ 8.26 (d, J = 7.2Hz, 2H), 7.54 (d, J = 8.9Hz, 2H), 7.48 (d, J = 7.2Hz, 2H), 7.01 (d, J = 8.9Hz, 2H), 3.87 (s, 3H). ^{13}C NMR ($\text{CDCl}_3/400$ MHz) δ 160.6, 139.2, 139.0, 128.3, 127.6, 123.0, 114.76, 55.4. HRMS-ESI+ m/e calcd for $\text{C}_{12}\text{H}_{12}\text{NO}_2$ ($\text{M}+\text{H}^+$) 202.0868, found 202.0863

Synthesis of 4-(4-nitrophenyl)pyridine *N*-oxide 19: In a 50 mL round bottomed flask, the 4-nitro(4-phenyl)pyridine (22 mg, 0.109 mmol) was dissolved in 10 mL of water and 10 mL of 2-butanone. Then, sodium bicarbonate was added (276 mg, 3.28 mmol) and the mixture was stirred vigorously. Oxone® is added in small portions (202 mg, 0.328 mmol) and the reaction was stirred at room temperature for three hours. Then 50 mL of brine were added and the reaction was extracted three times with

chloroform. The organic layers are combined, dried over sodium sulfate and concentrated under reduced pressure to afford the *N*-oxide as yellow needles (20 mg, yield 85%). ¹H NMR (CDCl₃/500 MHz) δ 8.37 (d, J = 8.3Hz, 2H), 8.32 (d, J = 6.1Hz, 2H), 7.77 (d, J = 8.3Hz, 2H), 7.57 (d, J = 6.1Hz, 2H). ¹³C NMR (CDCl₃/100 MHz) δ 160.5, 139.2, 139.1, 128.3, 127.6, 123.0, 114.7. HRMS-ESI- m/e calcd for C₁₁H₉N₂O₃ 217.0613, found 217.0618

ACKNOWLEDGMENT

We thank Gobierno de España MINECO (CTQ2011-23014), Generalitat de Catalunya DURSI (2009SGR6868) and ICIQ Foundation for financial support. A.G. thanks MINECO for a FPU fellowship. We also thank Professor Shannon Biros from the Chemistry Department of the Grand Valley State University, Allendale, Michigan for editing this manuscript

SUPPORTING INFORMATION PARAGRAPH

¹H and ¹³C-NMR spectra of the synthesized compounds, ¹H-NMR spectra registered during the variable temperature experiments, ¹H NMR spectra acquired in the binding studies, fits of the ITC titration data, figures of the X-ray crystal structures discussed in the text but not shown in the manuscript and X-ray crystallographic files of **2b**, **8**, **10**, **12**, **16**⊂**8**, **17**⊂**12**, **18**⊂**12** and **19**⊂**12**. This material is available free of charge via the Internet at <http://pubs.acs.org>.

REFERENCES

- ¹ Moran, J. R.; Karbach, S.; Cram, D. J., *J. Am. Chem. Soc.*, **1982**, *104*, 5826-5828.
- ² Moran, J. R.; Ericson, J. L.; Dalcanale, E.; Bryant, J. A.; Knobler, C. B.; Cram, D. J., *J. Am. Chem. Soc.*, **1991**, *113*, 5707-5714.
- ³ Dalcanale, E.; Soncini, P.; Bacchilega, G.; Ugozzoli, F., *J. Chem. Soc., Chem. Commun.*, **1989**, 500-502.

- ⁴ Soncini, P.; Bonsignore, S.; Dalcanale, E.; Ugozzoli, F., *J. Org. Chem.*, **1992**, *57*, 4608-4612.
- ⁵ Rieth, S.; Hermann, K.; Wang, B. Y.; Badjic, J. D., *Chem. Soc. Rev.*, **2011**, *40*, 1609-1622.
- ⁶ Rudkevich, D. M.; Rebek, J., *Eur. J. Org. Chem.*, **1999**, 1991-2005.
- ⁷ Korner, S. K.; Tucci, F. C.; Rudkevich, D. M.; Heinz, T.; Rebek, J., *Chem. Eur. J.*, **2000**, *6*, 187-195.
- ⁸ Heinz, T.; Rudkevich, D. M.; Rebek, J., *Nature*, **1998**, *394*, 764-766.
- ⁹ Liu, X. J.; Warmuth, R., *J. Am. Chem. Soc.*, **2006**, *128*, 14120-14127.
- ¹⁰ Biavardi, E.; Tudisco, C.; Maffei, F.; Motta, A.; Massera, C.; Condorelli, G. G.; Dalcanale, E., *Proc. Natl. Acad. Sci. U. S. A.*, **2012**, *109*, 2263-2268.
- ¹¹ Gissot, A.; Rebek, J., *J. Am. Chem. Soc.*, **2004**, *126*, 7424-7425.
- ¹² Pochorovski, I.; Ebert, M. O.; Gisselbrecht, J. P.; Boudon, C.; Schweizer, W. B.; Diederich, F., *J. Am. Chem. Soc.*, **2012**, *134*, 14702-14705.
- ¹³ Pochorovski, I.; Boudon, C.; Gisselbrecht, J. P.; Ebert, M. O.; Schweizer, W. B.; Diederich, F., *Angew. Chem., Int. Ed.*, **2012**, *51*, 262-266.
- ¹⁴ Renslo, A. R.; Rebek, J., *Angew. Chem., Int. Ed.*, **2000**, *39*, 3281-+.
- ¹⁵ Hooley, R. J.; Restorp, P.; Iwasawa, T.; Rebek, J., *J. Am. Chem. Soc.*, **2007**, *129*, 15639-15643.
- ¹⁶ Xiao, S. X.; Ajami, D.; Rebek, J., *Chem. Commun.*, **2010**, *46*, 2459-2461.
- ¹⁷ Lucking, U.; Rudkevich, D. M.; Rebek, J., *Tetrahedron Lett.*, **2000**, *41*, 9547-9551.
- ¹⁸ Gale, P. A.; Sessler, J. L.; Kral, V.; Lynch, V., *J. Am. Chem. Soc.*, **1996**, *118*, 5140-5141.
- ¹⁹ Anzenbacher, P.; Jursikova, K.; Lynch, V. M.; Gale, P. A.; Sessler, J. L., *J. Am. Chem. Soc.*, **1999**, *121*, 11020-11021.

- ²⁰ Gil-Ramirez, G.; Benet-Buchholz, J.; Escudero-Adan, E. C.; Ballester, P., *J. Am. Chem. Soc.*, **2007**, *129*, 3820-3821.
- ²¹ Ciardi, M.; Tancini, F.; Gil-Ramirez, G.; Escudero-Adan, E. C.; Massera, C.; Dalcanale, E.; Ballester, P., *J. Am. Chem. Soc.*, **2012**, *134*, 13121-13132.
- ²² Lippmann, T.; Wilde, H.; Dalcanale, E.; Mavilla, L.; Mann, G.; Heyer, U.; Spera, S., *J. Org. Chem.*, **1995**, *60*, 235-242.
- ²³ Jacopoizzi, P.; Dalcanale, E.; Spera, S.; Chrisstoffels, L. A. J.; Reinhoudt, D. N.; Lippmann, T.; Mann, G., *J. Chem. Soc., Perkin Trans. 2*, **1998**, 671-677.
- ²⁴ Dionisio, M.; Oliviero, G.; Menozzi, D.; Federici, S.; Yebeutchou, R. M.; Schmidtchen, F. P.; Dalcanale, E.; Bergese, P., *J. Am. Chem. Soc.*, **2012**, *134*, 2392-2398.
- ²⁵ Delangle, P.; Mulatier, J. C.; Tinant, B.; Declercq, J. P.; Dutasta, J. P., *Eur. J. Org. Chem.*, **2001**, 3695-3704.
- ²⁶ Melegari, M.; Suman, M.; Pirondini, L.; Moiani, D.; Massera, C.; Ugozzoli, F.; Kalenius, E.; Vainiotalo, P.; Mulatier, J. C.; Dutasta, J. P.; Dalcanale, E., *Chem. Eur. J.*, **2008**, *14*, 5772-5779.
- ²⁷ Slovak, S.; Evan-Salem, T.; Cohen, Y., *Org. Lett.*, **2010**, *12*, 4864-4867.
- ²⁸ Purse, B. W.; Rebek, J., *Proc. Natl. Acad. Sci. U. S. A.*, **2005**, *102*, 10777-10782.
- ²⁹ Moran, J. R.; Ericson, J. L.; Dalcanale, E.; Bryant, J. A.; Knobler, C. B.; Cram, D. J., *J. Am. Chem. Soc.*, **1991**, *113*, 5707-5714.
- ³⁰ SCIGRESS,V 3.0.0 Copyright 208-2014 Fujitsu Limited,
<http://www.fujitsu.com/global/services/solutions/tc/hpc/app/scigress/>
- ³¹ Becke, A. D., *Phys. Rev. A*, **1988**, *38*, 3098-3100.

- ³² Perdew, J. P., *Phys. Rev B.*, **1986**, *33*, 8822-8824.
- ³³ Grimme, S.; Antony, J.; Ehrlich, S.; Krieg, H., *J. Chem. Phys.*, **2010**, *132*, 154104.
- ³⁴ Ahlrichs, R.; Bär, M.; Häser, M.; Horn, H.; Kölmel, C., *Chem. Phys. Lett.*, **1989**, *162*, 165-169.
- ³⁵ Szumna, A., *Chem. Soc. Rev.*, **2010**, *39*, 4274-4285.
- ³⁶ Szumna, A., *Org. Biomol. Chem.*, **2007**, *5*, 1358-1368.
- ³⁷ Buckley, B. R.; Boxhall, J. Y.; Page, P. C. B.; Chan, Y. H.; Elsegood, M. R. J.; Heaney, H.; Holmes, K. E.; McIlldowie, M. J.; McKee, V.; McGrath, M. J.; Mocerino, M.; Poulton, A. M.; Sampler, E. P.; Skelton, B. W.; White, A. H., *Eur. J. Org. Chem.*, **2006**, 5117-5134.
- ³⁸ Stevens, M.; Pannecouque, C.; De Clercq, E.; Balzarini, J., *Biochem. Pharmacol.*, **2006**, *71*, 1122-1135.
- ³⁹ Balzarini, J.; Stevens, M.; Andrei, G.; Snoeck, R.; Strunk, R.; Pierce, J. B.; Lacadie, J. A.; De Clercq, E.; Pannecouque, C., *Helv. Chim. Acta*, **2002**, *85*, 2961-2974.
- ⁴⁰ Verdejo, B.; Gil-Ramirez, G.; Ballester, P., *J. Am. Chem. Soc.*, **2009**, *131*, 3178-3179.
- ⁴¹ Espelt, M.; Ballester, P., *Org. Lett.*, **2012**, *14*, 5708-5711.
- ⁴² Gil-Ramirez, G.; Chas, M.; Ballester, P., *J. Am. Chem. Soc.*, **2010**, *132*, 2520-2521.
- ⁴³ Adriaenssens, L.; Ballester, P., *Chem. Soc. Rev.*, **2013**, *42*, 3261-3277.
- ⁴⁴ Roncucci, P.; Pirondini, L.; Paderni, G.; Massera, C.; Dalcanale, E.; Azov, V. A.; Diederich, F., *Chem. Eur. J.*, **2006**, *12*, 4775-4784.
- ⁴⁵ The ratio 0.85:1 established between the concentrations of DMF and **12** was derived from manually fitting the value of the molar ratio for the inflexion point in the first sigmoidal curve.

⁴⁶ Kazimierczuk, Z.; Dudycz, L.; Stolarski, R.; Shugar, D., *J. Carbohydr. Nucleos. Nucleot.*, **1981**, 8, 101-117.